

## Communication

# Aqueous Zn//Zn(CF<sub>3</sub>SO<sub>3</sub>)<sub>2</sub>//Na<sub>3</sub>V<sub>2</sub>(PO<sub>4</sub>)<sub>3</sub> batteries with simultaneous Zn<sup>2+</sup>/Na<sup>+</sup> intercalation/de-intercalation



Ping Hu<sup>a</sup>, Ting Zhu<sup>a</sup>, Xuanpeng Wang<sup>a</sup>, Xufeng Zhou<sup>b</sup>, Xiujuan Wei<sup>a</sup>, Xuhui Yao<sup>a</sup>, Wen Luo<sup>a</sup>, Changwei Shi<sup>a</sup>, Kwadwo Asare Owusu<sup>a</sup>, Liang Zhou<sup>a,\*</sup>, Liqiang Mai<sup>a,\*</sup>

<sup>a</sup> State Key Laboratory of Advanced Technology for Materials Synthesis and Processing, International School of Materials Science and Engineering, Wuhan University of Technology, Wuhan 430070, China

<sup>b</sup> Ningbo Institute of Materials, Chinese Academy of Sciences, Ningbo 315000, China

## ARTICLE INFO

## Keywords:

Aqueous zinc-ion battery  
NASICON structure  
Na<sub>3</sub>V<sub>2</sub>(PO<sub>4</sub>)<sub>3</sub>  
Zn<sup>2+</sup>/Na<sup>+</sup> intercalation/de-intercalation  
Discharge plateau

## ABSTRACT

Aqueous zinc-ion batteries (ZIBs) represent an attractive choice for stationary energy storage. Its widespread application relies on the development of novel, reliable cathode materials. Herein, we find NASICON structured Na<sub>3</sub>V<sub>2</sub>(PO<sub>4</sub>)<sub>3</sub> manifests simultaneous Zn<sup>2+</sup>/Na<sup>+</sup> intercalation/de-intercalation in a single component electrolyte (2.0 M Zn(CF<sub>3</sub>SO<sub>3</sub>)<sub>2</sub>). The Na<sub>3</sub>V<sub>2</sub>(PO<sub>4</sub>)<sub>3</sub>/rGO microspheres prepared by spray drying deliver a high specific capacity of 114 mAh g<sup>-1</sup> with an average discharge platform of 1.23 V at 50 mA g<sup>-1</sup>. Impressively, a high capacity of 74 mAh g<sup>-1</sup> can be obtained after 200 cycles at 500 mA g<sup>-1</sup>. These excellent electrochemical performances can be ascribed to the stable and open NASICON framework, fast ion diffusion, as well as continuous electron transport. This work sheds light on the development of secondary batteries with hybrid ion intercalation/de-intercalation behaviors using a single component electrolyte.

## 1. Introduction

Aqueous zinc-ion batteries (ZIBs), which is comprised of a metallic Zn anode, an aqueous electrolyte, and a cathode for Zn<sup>2+</sup> accommodation, have been identified as a promising choice for stationary energy storage. The virtues of Zn anode include low cost, high theoretical capacity (820 mAh g<sup>-1</sup>), and feasible redox potential (−0.78 V vs. standard hydrogen electrode) in aqueous electrolytes [1–8]. The cathode materials for aqueous ZIBs can be generally categorized into three families: Mn-based materials [9–15], Prussian blue [16,17], and V-based materials [18–23]. However, the rapid capacity decay of MnO<sub>2</sub> and the limited capacity (~ 50 mAh g<sup>-1</sup>) of Prussian blue analogs hinder their extensive application [16].

V-based materials, such as VO<sub>2</sub>, V<sub>2</sub>O<sub>5</sub>·xH<sub>2</sub>O, H<sub>2</sub>V<sub>3</sub>O<sub>8</sub>, Na<sub>2</sub>V<sub>6</sub>O<sub>16</sub>·xH<sub>2</sub>O, Mg<sub>x</sub>V<sub>2</sub>O<sub>5</sub>·nH<sub>2</sub>O, Zn<sub>3</sub>V<sub>2</sub>O<sub>7</sub>(OH)<sub>2</sub>·2H<sub>2</sub>O, LiV<sub>3</sub>O<sub>8</sub>, and VS<sub>2</sub>, have been extensively investigated as ZIB cathode materials [18–31]. For example, Yan et al. reported a water-lubricated intercalation cathode material (V<sub>2</sub>O<sub>5</sub>·nH<sub>2</sub>O) with a specific capacity of 372 mAh g<sup>-1</sup> and an average discharge plateau at ~ 0.6 V [18]. Kim et al. designed a layered-type LiV<sub>3</sub>O<sub>8</sub> cathode, which delivered a specific capacity of 172 mAh g<sup>-1</sup> with an average voltage platform of ~ 0.72 V [20]. Alshareef et al. prepared a zinc pyrovanadate

(Zn<sub>3</sub>V<sub>2</sub>O<sub>7</sub>(OH)<sub>2</sub>·2H<sub>2</sub>O) nanowire cathode, which manifested a capacity of 213 mAh g<sup>-1</sup> with an average voltage platform of ~ 0.7 V [19]. Although the V-based materials display relatively high specific capacities, they usually suffer from low discharge plateaus, making them less competitive in energy density.

NASICON (Na ion super ionic conductor) structured Na<sub>3</sub>V<sub>2</sub>(PO<sub>4</sub>)<sub>3</sub> (NVP) is a well-known cathode material for alkali/multivalent ion batteries [32–36]. Recently, Huang et al. firstly demonstrated that the NVP can be employed as a ZIB cathode material. In aqueous Zn(CH<sub>3</sub>COO)<sub>2</sub> electrolyte, two Na<sup>+</sup> were extracted from the NVP framework during the first charge, after which Zn<sup>2+</sup> intercalated into/de-intercalated from the lattice reversibly, leading to a reversible capacity of 97 mAh g<sup>-1</sup> and a discharge platform at 1.1 V vs. Zn<sup>2+</sup>/Zn [21]. When applied in hybrid Zn//NVP batteries with aqueous CH<sub>3</sub>COONa/Zn(CH<sub>3</sub>COO)<sub>2</sub> electrolyte, the Na<sup>+</sup> could be extracted from/insert into the NVP framework reversibly, giving rise to a capacity of 92 mAh g<sup>-1</sup> at a high discharge plateau of 1.42 V vs. Zn<sup>2+</sup>/Zn [37]. However, to the best of our knowledge, the simultaneous intercalation/de-intercalation of Zn<sup>2+</sup>/Na<sup>+</sup> into/from NVP in a single component electrolyte has not been realized.

Herein, we demonstrate the simultaneous Zn<sup>2+</sup>/Na<sup>+</sup> intercalation/de-intercalation behavior of Na<sub>3</sub>V<sub>2</sub>(PO<sub>4</sub>)<sub>3</sub>@reduced graphene oxide

\* Corresponding authors.

E-mail addresses: [liangzhou@whut.edu.cn](mailto:liangzhou@whut.edu.cn) (L. Zhou), [mlq518@whut.edu.cn](mailto:mlq518@whut.edu.cn) (L. Mai).

<https://doi.org/10.1016/j.nanoen.2019.01.068>

Received 30 October 2018; Received in revised form 19 January 2019; Accepted 26 January 2019

Available online 28 January 2019

2211-2855/ © 2019 Elsevier Ltd. All rights reserved.

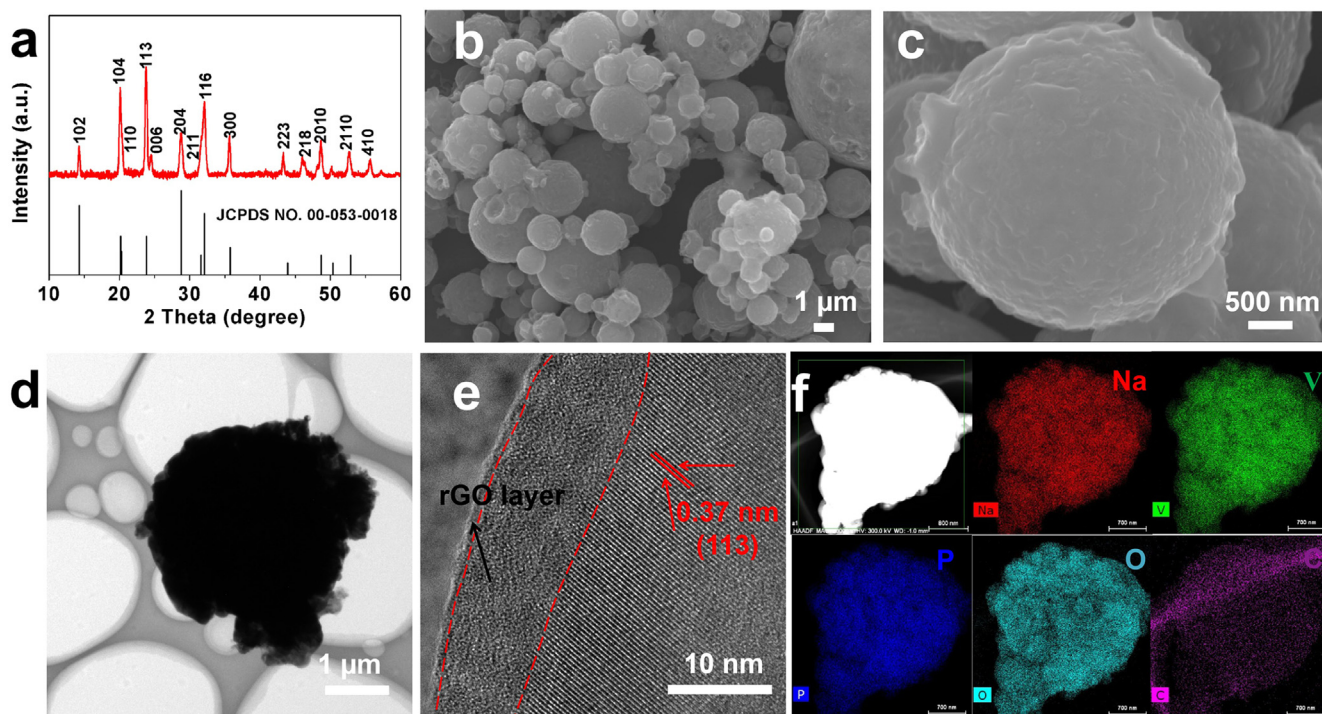


Fig. 1. XRD pattern (a), SEM (b, c), TEM (d), HRTEM images (e), and elemental mappings (f) of NVP@rGO.

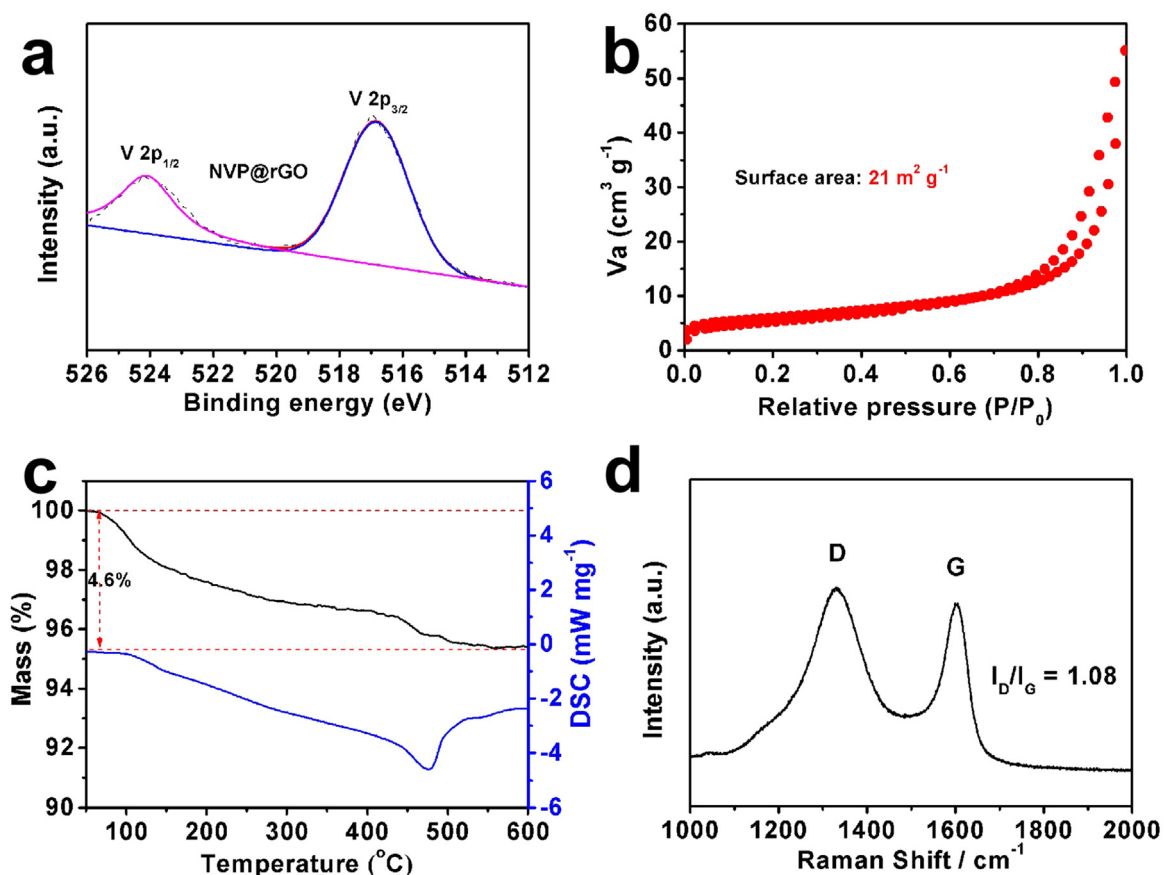
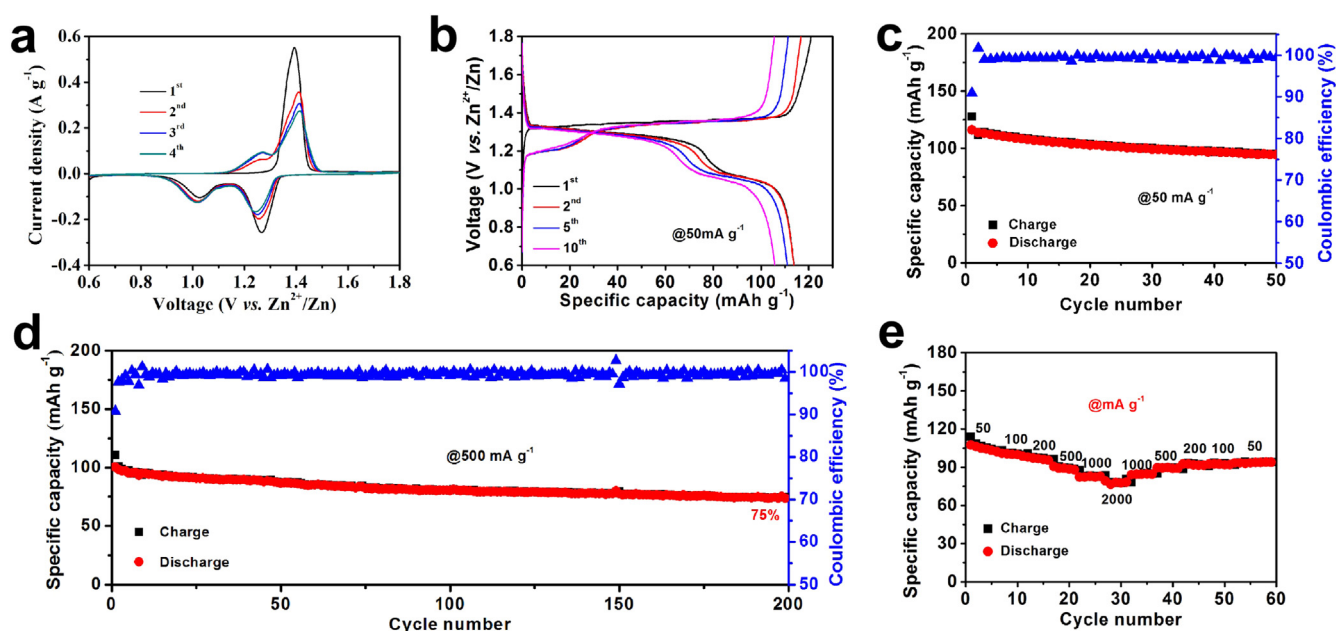


Fig. 2. (a) V2p XPS spectrum and (b) N<sub>2</sub> adsorption-desorption isotherm, (c) TGA curve, (d) Raman spectrum of NVP@rGO.



**Fig. 3.** Electrochemical performances NVP@rGO in the electrochemical window of 0.6 – 1.8 V vs. Zn<sup>2+</sup>/Zn. (a) CV profiles at a scan rate of 0.1 mV s<sup>-1</sup>. (b) Charge/discharge curves at 50 mA g<sup>-1</sup>. (c – d) Cycling performance at 50 and 500 mA g<sup>-1</sup>. (e) Rate performance at various current densities ranging from 50 to 2000 mA g<sup>-1</sup>.

(NVP@rGO) in a single component 2.0 M Zn(CF<sub>3</sub>SO<sub>3</sub>)<sub>2</sub> electrolyte. The NVP@rGO delivers a high specific capacity of 114 mAh g<sup>-1</sup> with an average discharge platform of 1.23 V in the potential window of 0.6 – 1.8 V vs. Zn<sup>2+</sup>/Zn. Long-term cycling ability (75% capacity retention after 200 cycles at 500 mA g<sup>-1</sup>) and superior rate capability (82 mAh g<sup>-1</sup> at 2000 mA g<sup>-1</sup>) is also achieved.

## 2. Experimental section

### 2.1. Synthesis of NVP@rGO microspheres

In a typical synthesis, 6 mmol of Na<sub>2</sub>CO<sub>3</sub>, 4 mmol of V<sub>2</sub>O<sub>5</sub>, and 12 mmol of NH<sub>4</sub>H<sub>2</sub>PO<sub>4</sub> were added into 90 mL of distilled water and stirred at 70 °C for 30 min. Then, 60 mL of rGO (2 mg mL<sup>-1</sup>) was added and stirred for another 10 min. Then, the suspension was spray-dried by using a BUCHI Mini Spray Dryer B-290 to prepare the NVP@rGO precursor. After annealing the precursor at 750 °C in Ar for 4 h, the NVP@rGO was obtained.

### 2.2. Structure characterization

*Ex-situ* X-ray diffraction (XRD) experiments during electrochemical measurement of the Zn//Zn(CF<sub>3</sub>SO<sub>3</sub>)<sub>2</sub>/NVP@rGO aqueous hybrid-ion batteries were performed on a D8 Discover X-ray diffractometer with a nonmonochromated Cu Kα X-ray source (2θ range: 10 – 60°). Field-emission scanning electron microscopy (FESEM) images were collected using a JSM-7001F microscope at an acceleration voltage of 10 kV. Transmission electron microscopy (TEM) and high-resolution TEM images (HRTEM) were recorded with a JSM-2100F STEM/EDS microscope. The X-ray photoelectron (XPS) spectra were recorded on a Shimadzu Axis Ultra spectrometer with an Mg Kα = 1253.6 eV excitation source. The Brunauer-Emmett-Teller (BET) surface area was calculated from nitrogen adsorption-desorption isotherms collected at 77 K using a Tristar-3020 instrument. Thermogravimetric analysis (TGA) and differential scanning calorimeter (DSC) curves were conducted by using a Netzsch STA 449 C simultaneous analyzer.

### 2.3. Electrochemical characterization

The cathode was fabricated by pressing a slurry containing NVP@rGO (70 wt%), acetylene black (20 wt%), and polyvinylidene fluoride (10 wt%) onto a titanium foil and dried under vacuum at 70 °C for 12 h. Zn foil with a thickness of 0.25 mm was used as the anode. Aqueous zinc trifluoromethanesulfonate (2 M Zn(CF<sub>3</sub>SO<sub>3</sub>)<sub>2</sub>) solution was used as the electrolyte. 2016-type coin cells were assembled by sandwiching a filter paper (Whatman grade A) wetted with an electrolyte between the prepared cathode and zinc foil anode. Cyclic voltammetry (CV) and electrochemical impedance spectroscopy (EIS) were tested with an electrochemical workstation (Autolab PGSTAT 302 N). Galvanostatic intermittent titration technique (GITT) test was performed at a current density of 16 mA g<sup>-1</sup> on a LAND CT2001A multichannel battery testing system.

## 3. Results and discussions

The NVP@rGO microspheres are synthesized by a facile spray-drying-assisted method. The XRD pattern of obtained NVP@rGO (Fig. 1a) agrees well with the NASICON structured Na<sub>3</sub>V<sub>2</sub>(PO<sub>4</sub>)<sub>3</sub> with a R3c space group (JCPDS 053-0018). SEM images (Fig. 1b, c) show that the NVP@rGO is composed of microspheres with diameters ranging from hundreds of nanometers to several micrometers. TEM image further confirms the microspherical morphology of NVP@rGO (Fig. 1d). The (113) lattice fringe of NVP with the interplanar spacing of 0.37 nm can be clearly observed under the HRTEM image (Fig. 1e). Besides, a thin amorphous layer, which might be the rGO, can also be observed at the surface (Fig. 1e). Energy-dispersive X-ray spectroscopy (EDS) elemental mappings of the as-prepared NVP@rGO show that the Na, V, P, O, and C elements are homogeneously distributed within the sample (Fig. 1f).

To explore the V valence states of NVP@rGO, the V2p XPS spectrum is collected (Fig. 2a). The V2p core level spectrum displays a spin-orbit doublet with binding energies of 517.0 (2p<sub>3/2</sub>) and 524.2 eV (2p<sub>1/2</sub>). The binding energies match well with those of Na<sub>3</sub>V<sub>2</sub>(PO<sub>4</sub>)<sub>3</sub>, Li<sub>3</sub>V<sub>2</sub>(PO<sub>4</sub>)<sub>3</sub>, and Na<sub>3</sub>V<sub>1.7</sub>Fe<sub>x</sub>(PO<sub>4</sub>)<sub>3</sub> [32, 38–40]. N<sub>2</sub> sorption result shows that the NVP@rGO possesses a specific BET surface area of 21 m<sup>2</sup> g<sup>-1</sup> (Fig. 2b). TGA is used to study the rGO content. The NVP@rGO

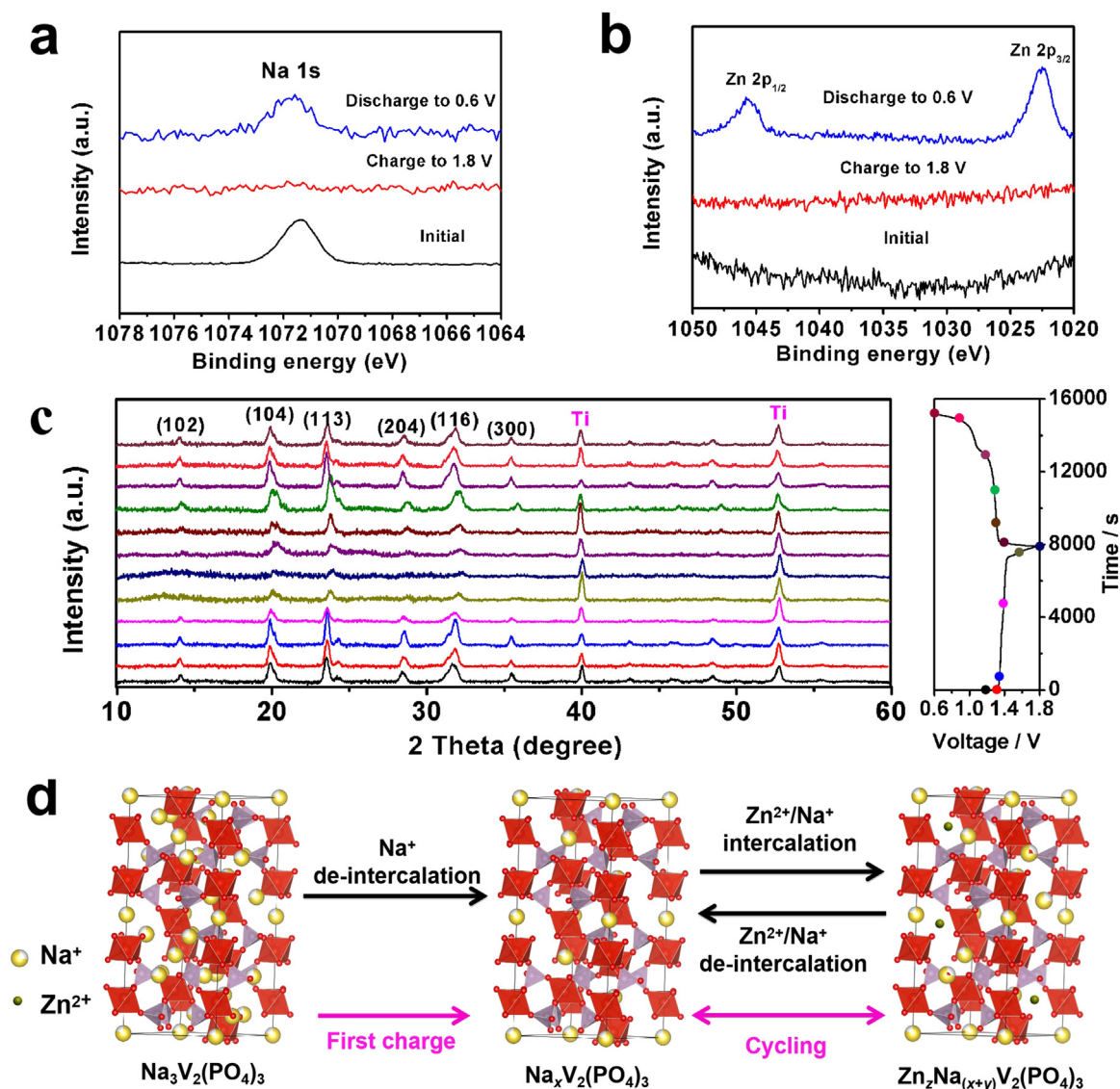


Fig. 4. XPS spectra of (a) Na 1s and (b) Zn 2p of the NVP@rGO in its original, charged, and discharged states; (c) *Ex-situ* XRD patterns of the NVP@rGO collected at different electrochemical states in 2 M  $\text{Zn}(\text{CF}_3\text{SO}_3)_2$  electrolyte at  $100 \text{ mA g}^{-1}$ ; (d) Schematic illustrations of ions de-intercalation/intercalation from/into the NVP@rGO during charge/discharge processes.

shows a weight loss of  $\sim 4.6\%$  below  $600^\circ\text{C}$  (Fig. 2 c), which is attributed to the burning-off of rGO. The Raman spectrum of NVP@rGO (Fig. 2d) displays two characteristic bands of D-band (disorder-induced phonon mode) and G-band (graphite), which are located at  $1330 \text{ cm}^{-1}$  and  $1598 \text{ cm}^{-1}$ , respectively. Meanwhile, the  $I_D$  to  $I_G$  ratio is 1.08.

The electrochemical properties of the NVP@rGO for ZIBs are investigated by CV and galvanostatic charge-discharge. During the initial anodic scan, a strong oxidation peak can be observed at  $1.39 \text{ V}$ , which is attributed to the de-intercalation of  $\text{Na}^+$  from the NVP framework (Fig. 3a). The subsequent cathodic scan displays two reduction peaks at  $1.26$  and  $1.02 \text{ V}$ , which are caused by the co-intercalation of  $\text{Na}^+$  and  $\text{Zn}^{2+}$  into the  $\text{Na}_x\text{V}_2(\text{PO}_4)_3$  framework, respectively. In the second anodic scan, a new oxidation peak at  $1.26 \text{ V}$  appears, which is attributable to the  $\text{Zn}^{2+}$  de-intercalation from the material. From the second cycle onward, two pairs of reduction/oxidation peaks located at  $\sim 1.26/1.39$  and  $1.02/1.26 \text{ V}$  can be clearly observed, which are caused by the intercalation/de-intercalation of  $\text{Na}^+$  and  $\text{Zn}^{2+}$ , respectively. In addition, the redox peaks associated with  $\text{Zn}^{2+}$  intercalation/de-intercalation processes strengthen with cycling, accompanying the gradual weakening of  $\text{Na}^+$  intercalation/de-intercalation redox peaks (Fig. 3a).

Representative charge-discharge profiles of NVP@rGO at  $50 \text{ mA g}^{-1}$

are displayed in Fig. 3b. Agreeing well with the CV results, the first charge process shows only one charge plateaus. For the subsequent discharge processes, two plateaus can be observed at  $\sim 1.3$  and  $1.05 \text{ V}$ , corresponding to the intercalation of  $\text{Na}^+$  and  $\text{Zn}^{2+}$ . The average discharge platform is determined to be  $\sim 1.23 \text{ V}$ . At a current density of  $50 \text{ mA g}^{-1}$ , the NVP@rGO delivers an initial capacity of  $114 \text{ mAh g}^{-1}$ , among which  $83 \text{ mAh g}^{-1}$  is contributed from the  $\text{Na}^+$  intercalation and  $31 \text{ mAh g}^{-1}$  is from the  $\text{Zn}^{2+}$  intercalation (Fig. S1). After 50 cycles at  $50 \text{ mA g}^{-1}$ , the capacity fades slowly to  $\sim 95 \text{ mAh g}^{-1}$  (Fig. 3c). At  $500 \text{ mA g}^{-1}$ , the NVP@rGO shows an initial discharge capacity of  $101 \text{ mAh g}^{-1}$  and maintains  $75\%$  ( $\sim 76 \text{ mAh g}^{-1}$ ) after 200 cycles (Fig. 3d). Besides the excellent cycling performance, the NVP@rGO also demonstrates superior rate capability (Fig. 3e). The NVP@rGO delivers high discharge capacities of  $107, 102, 99, 96, 88,$  and  $82 \text{ mAh g}^{-1}$  at  $50, 100, 200, 500, 1000,$  and  $2000 \text{ mA g}^{-1}$ , respectively (Fig. 3e and S2). When the current density is reduced to  $50 \text{ mA g}^{-1}$ , around  $93\%$  of the initial discharge capacity can be recovered.

To explain the superior rate performance of NVP@rGO, GITT and EIS are employed to explore the ion diffusion coefficient and charge transfer resistance (Fig. S3 and S4). Although the divalent nature of  $\text{Zn}^{2+}$ , the  $\text{Zn}^{2+}$  diffusion coefficient determined by GITT is as high as

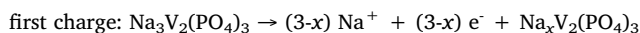
ca.  $10^{-8}$  to  $10^{-9}$   $\text{cm}^2 \text{s}^{-1}$ , even higher than that of  $\text{Na}^+$  diffusion coefficient ( $\sim 10^{-10}$  to  $10^{-9}$   $\text{cm}^2 \text{s}^{-1}$ ). From the Nyquist plots, the charge transfer resistance of the NVP@rGO cathode is determined to be  $80 \Omega$ . The GITT and EIS results clearly demonstrate the fast kinetics of ion/electron transport in the NVP@rGO cathode, which is beneficial for the rate performance.

To elucidate the charge storage mechanism, *ex-situ* XPS and XRD are performed. The XPS spectra of the NVP/rGO in its original state, charged state (charged to 1.8 V), and discharged state (discharged to 0.6 V) are shown in Fig. 4a–b and Fig. S5. In the original state, the Na 1s peak located at 1077 eV can be clearly discerned, while there is no signal of Zn. After charging to 1.8 V, the intensity of the Na 1s peak decreases significantly, indicating the extraction of  $\text{Na}^+$  from the NVP@rGO; still, there is no signal for Zn. When discharged to 0.6 V, both Na and Zn can be detected in the sample. The *ex-situ* XPS results unambiguously demonstrate the co-intercalation of  $\text{Zn}^{2+}$  and  $\text{Na}^+$  into the  $\text{Na}_x\text{V}_2(\text{PO}_4)_3$  framework during the subsequent discharge process.

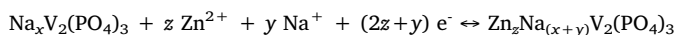
The crystalline structure of NVP@rGO during the charge/discharge processes is monitored by *ex-situ* XRD (Fig. 4c). During the first charge ( $\text{Na}^+$  extraction) process, the (116) diffraction located at  $\sim 32.1^\circ$  shifts towards higher  $2\theta$  positions and weakens in intensity. A similar trend can be observed for the (113) diffraction located at  $\sim 23.8^\circ$ . Even for the sample under a fully charged state, its XRD pattern resembles that of the original NVP@rGO despite its weak intensity, suggesting the excellent structural stability of the NVP NASICON framework. Upon discharge to 1.2 V, both the (116) and (113) diffractions shift to lower  $2\theta$  positions, which is caused by the  $\text{Na}^+$  intercalation. Upon further discharge to 0.6 V, the (211) and (113) diffractions shift rightward slightly, which is caused by the  $\text{Zn}^{2+}$  intercalation. Besides, the diffractions strengthen in intensity during the discharge.

To study the role of de-intercalated  $\text{Na}^+$  during the subsequent discharge/charge processes, the NVP@rGO is charged to 1.8 V, washed thoroughly with deionized water, and then assembled with a Zn anode and  $\text{Zn}(\text{CF}_3\text{SO}_3)_2$  electrolyte for the electrochemical performance test. Due to the absence of  $\text{Na}^+$  in the electrolyte, the obtained  $\text{Na}_x\text{V}_2(\text{PO}_4)_3$ @rGO exhibits only one discharge platform at  $\sim 1.15$  V, while no discharge platform at  $\sim 1.3$  V can be detected (Fig. S6 and S7). The result clearly demonstrates that the discharge plateau at  $\sim 1.15$  V is caused by  $\text{Zn}^{2+}$  intercalation while the discharge plateau at  $\sim 1.3$  V is caused by  $\text{Na}^+$  intercalation.

Based on the above results and discussions, the electrochemical reactions happen in the NVP@rGO cathode can be described as follows (Fig. 4d):



the subsequent discharge/charge:



When compared to the recently reported aqueous Li/Na/Zn-ion batteries, the Zn//Zn( $\text{CF}_3\text{SO}_3$ )<sub>2</sub>/NVP@rGO battery with  $\text{Zn}^{2+}$  and  $\text{Na}^+$  co-intercalation behavior in this study manifests comparable or even better electrochemical performance in terms of energy density and power density (Fig. S8) [19–21,41–48], demonstrating its great potential in stationary energy storage.

#### 4. Conclusion

In summary, we design a  $\text{Na}_3\text{V}_2(\text{PO}_4)_3$ /reduced graphene oxide (NVP@rGO) composite cathode material for aqueous zinc-ion batteries. The obtained NVP@rGO demonstrates simultaneous  $\text{Zn}^{2+}/\text{Na}^+$  intercalation/de-intercalation behaviors in a single component electrolyte (2 M Zn( $\text{CF}_3\text{SO}_3$ )<sub>2</sub>). The NVP@rGO manifests a high specific capacity of 114 mAh  $\text{g}^{-1}$  with an average discharge plateaus at 1.23 V vs.  $\text{Zn}^{2+}/\text{Zn}$ .

Excellent cycling (74 mAh  $\text{g}^{-1}$  after 200 cycles at 500 mA  $\text{g}^{-1}$ ) and rate performances (82 mAh  $\text{g}^{-1}$  at 2000 mA  $\text{g}^{-1}$ ) are also obtained. These excellent electrochemical performances can be ascribed to the stable and open NASICON framework, fast ion diffusion, as well as continuous electron transport. This work sheds light on the development of secondary batteries with hybrid ion intercalation/de-intercalation behaviors using a single component electrolyte.

#### Acknowledgements

This work was supported by the National Key Research and Development Program of China (2016YFA0202603), the National Natural Science Foundation of China (51521001, 21673171).

#### Appendix A. Supporting information

Supplementary data associated with this article can be found in the online version at doi:10.1016/j.nanoen.2019.01.068.

#### References

- [1] N. Zhang, F.Y. Cheng, J.X. Liu, L.B. Wang, X.H. Long, X.S. Liu, F.J. Li, J. Chen, Nat. Commun. 8 (2017) 405.
- [2] H.L. Pan, Y.Y. Shao, P.F. Yan, Y.W. Cheng, K.S. Han, Z.M. Nie, C.M. Wang, J.H. Yang, X.L. Li, P. Bhattacharya, K.T. Muller, J. Liu, Nat. Energy 1 (2016) 16039.
- [3] D. Kundu, B.D. Adams, V. Duffort, S.H. Vajargah, L.F. Nazar, Nat. Energy 1 (2016) 16119.
- [4] G.Z. Fang, J. Zhou, A.Q. Pan, S.Q. Liang, ACS Energy Lett. 3 (2018) 2480–2501.
- [5] A. Konarov, N. Voronina, J.H. Jo, Z. Bakonov, Y. Sun, S. Myung, ACS Energy Lett. 3 (2018) 2620–2640.
- [6] X.W. Wu, Y.H. Xiang, Q.J. Peng, X.S. Wu, Y.H. Li, F. Tang, R.C. Song, Z.X. Liu, Z.Q. He, X.M. Wu, J. Mater. Chem. A 5 (2017) 17990–17997.
- [7] K. Lu, B. Song, Y.X. Zhang, H.Y. Ma, J.T. Zhang, J. Mater. Chem. A 5 (2017) 23628–23633.
- [8] P. He, Y.L. Qian, X. Xu, M.Y. Yan, W. Yang, Q.Y. An, L. He, Small 13 (2017) 1702551.
- [9] C.J. Xu, B.H. Li, H.D. Du, F.Y. Kang, Angew. Chem. Int. Ed. 51 (2012) 933–935.
- [10] B.Z. Jiang, C.J. Xu, C.L. Wu, L.B. Dong, J. Li, F.Y. Kang, Electrochim. Acta 229 (2017) 422–428.
- [11] S. Islam, M.H. Alfaruqi, V. Mathew, J. Song, S. Kim, S. Kim, J. Jo, J.P. Baboo, D.T. Pham, D.Y. Putro, Y. Sun, J. Kim, J. Mater. Chem. A 5 (2017) 23299–23309.
- [12] M.H. Alfaruqi, V. Mathew, J. Gim, S. Kim, J.J. Song, J. Baboo, S.H. Choi, J. Kim, Chem. Mater. 27 (2015) 3609–3620.
- [13] N. Zhang, F.Y. Cheng, Y.C. Liu, Q. Zhang, K.X. Lei, C.C. Chen, X.S. Liu, J. Chen, J. Am. Chem. Soc. 138 (2016) 12894–12901.
- [14] W. Sun, F. Wang, S. Hou, C.Y. Yang, X.L. Fan, Z.H. Ma, T. Gao, F.D. Han, R.Z. Hu, M. Zhu, C.S. Wang, J. Am. Chem. Soc. 139 (2017) 9775–9778.
- [15] S. Islam, M.H. Alfaruqi, J. Song, S. Kim, D.T. Pham, J. Jo, S. Kim, V. Mathew, J.P. Baboo, Z.L. Xiu, J. Kim, J. Energy Chem. 26 (2017) 815–819.
- [16] K. Lu, B. Song, Y.X. Zhang, H.Y. Ma, J.T. Zhang, J. Mater. Chem. A 5 (2017) 23628–23633.
- [17] L.Y. Zhang, L. Chen, X.F. Zhou, Z.P. Liu, Sci. Rep. 5 (2015) 18263.
- [18] M.Y. Yan, P. He, Y. Chen, S.Y. Wang, Q.L. Wei, K.N. Zhao, X. Xu, Q.Y. An, Y. Shuang, Y.Y. Shao, K.T. Muller, L.Q. Mai, J. Liu, J.H. Yang, Adv. Mater. 30 (2017) 1703725.
- [19] P. He, M.Y. Yan, G.B. Zhang, R.M. Sun, L.N. Chen, Q.Y. An, L.Q. Mai, Adv. Energy Mater. 7 (2017) 1601920.
- [20] M.H. Alfaruqi, V. Mathew, J. Song, S. Kim, S. Islam, D.T. Pham, J. Jo, S. Kim, J.P. Baboo, Z.L. Xiu, K.S. Lee, Y.K. Sun, J. Kim, Chem. Mater. 29 (2017) 1684–1694.
- [21] G.L. Li, Z. Yang, Y. Jiang, C.H. Jin, W. Huang, X. Ding, Y.H. Huang, Nano Energy 25 (2015) 211–217.
- [22] M.H. Alfaruqi, S. Islam, V. Mathew, J.J. Song, S.J. Kim, D.P. Tung, J. Jo, S. Kim, J.P. Baboo, Z.L. Xiu, J. Kim, Appl. Surf. Sci. 404 (2017) 435–442.
- [23] P. Senguttuvan, S.D. Han, S. Kim, A.L. Lipson, S. Tepavcevic, T.T. Fister, I.D. Bloom, A.K. Burrell, C.S. Johnson, Adv. Energy Mater. 6 (2016) 1600826.
- [24] C. Xia, J. Guo, Y.J. Lei, H.F. Liang, C. Zhao, H.N. Alshareef, Adv. Mater. 30 (2017) 1705580.
- [25] P. Hu, M.Y. Yan, T. Zhu, X.P. Wang, X.J. Wei, J.T. Li, L. Zhou, Z.H. Li, L.N. Chen, L.Q. Mai, ACS Appl. Mater. Interfaces 9 (2017) 42717–42722.
- [26] P. Hu, T. Zhu, X.P. Wang, X.J. Wei, M.Y. Yan, J.T. Li, W. Luo, W. Yang, W.C. Zhang, L. Zhou, L.Q. Mai, Nano Lett. 18 (2018) 1758–1763.
- [27] V. Soundharajan, B. Sambandan, S. Kim, M.H. Alfaruqi, D.Y. Putro, J. Jo, S. Kim, V. Mathew, Y.K. Sun, J. Kim, Nano Lett. 18 (2018) 2402–2410.
- [28] C. Xia, J. Guo, P. Li, X.X. Zhang, H.N. Alshareef, Angew. Chem. Int. Ed. 57 (2018) 1–7.
- [29] F.W. Ming, H.F. Liang, Y.J. Lei, S. Kandambeth, M. Eddaoudi, H.N. Alshareef, ACS Energy Lett. 3 (2018) 2602–2609.
- [30] J.W. Ding, Z.G. Du, L.Q. Gu, B. Li, L.Z. Wang, S.W. Wang, Y. Gong, S.B. Yang, Adv. Mater. 30 (2018) 1800762.

- [31] D. Kundu, S.H. Vajargah, L.W. Wan, B. Adams, D. Prentdergast, L.F. Nazar, *Energy Environ. Sci.* 11 (2018) 881–892.
- [32] Q.Y. An, F.Y. Xiong, Q.L. Wei, J.Z. Sheng, L. He, D.L. Ma, Y. Yao, L.Q. Mai, *Adv. Energy Mater.* 5 (2015) 1401963.
- [33] W.H. Ren, Z.P. Zheng, C. Xu, C.J. Niu, Q.L. Wei, Q.Y. An, K.N. Zhao, M.Y. Yan, M.S. Qin, L.Q. Mai, *Nano Energy* 25 (2016) 145–153.
- [34] Y.F. Li, Q.Y. An, Y.W. Cheng, Y.L. Liang, Y. Ren, C.J. Sun, H. Dong, Z.J. Tang, G.S. Li, Y. Yao, *Nano Energy* 34 (2017) 188–194.
- [35] X.H. Rui, W.P. Sun, C. Wu, Y. Yu, Q.Y. Yan, *Adv. Mater.* 27 (2015) 6670–6676.
- [36] Q. Zheng, H.M. Yi, X.F. Li, H.M. Zhang, *J. Energy Chem.* 27 (2018) 1597–1617.
- [37] G.L. Li, Z. Yang, Y. Jiang, W.X. Zhang, Y.H. Huang, *J. Power Sources* 308 (2016) 52–57.
- [38] M.J. Aragón, P. Lavela, G.F. Ortiz, J.L. Tirado, *J. Electrochem. Soc.* 162 (2015) 3077–3083.
- [39] J.C. Zeng, X.H. Li, Z.X. Wang, H.J. Guo, Q.Y. Hu, W.J. Peng, *J. Power Sources* 189 (2009) 476–479.
- [40] M.M. Ren, Z. Zhou, Y.Z. Li, X.P. Gao, J. Yan, *J. Power Sources* 162 (2006) 357–1362.
- [41] D. Bin, Y.P. Wen, Y.G. Wang, Y.Y. Xia, *J. Energy Chem.* 27 (2018) 1521–1535.
- [42] L.M. Suo, O. Borodin, W. Sun, X.L. Fan, C.Y. Yang, F. Wang, T. Gao, Z.H. Ma, M. Schroeder, A. von Cresce, S.M. Russell, M. Armand, A. Angell, K. Xu, C.S. Wang, *Angew. Chem. Int. Ed.* 55 (2016) 7136–7141.
- [43] Y.G. Wang, Y.Y. Xia, *J. Electrochem. Soc.* 153 (2006) A450–A454.
- [44] F. Wang, L.M. Suo, Y.J. Liang, C.Y. Yang, F.D. Han, T. Gao, W. Sun, C.S. Wang, *Adv. Energy Mater.* 7 (2017) 1600922.
- [45] Y.S. Wang, L.Q. Mu, J. Liu, Z.Z. Yang, X.Q. Yu, L. Gu, Y.S. Hu, H. Li, X.Q. Yang, L.Q. Chen, X.J. Huang, *Adv. Energy Mater.* 5 (2015) 1501005.
- [46] Z.G. Hou, X.N. Li, J.W. Liang, Y.C. Zhu, Y.T. Qian, *J. Mater. Chem. A* 3 (2015) 1400–1404.
- [47] H. Zhang, B.S. Qin, J. Han, S. Passerini, *ACS Energy Lett.* 3 (2018) 1769–1770.
- [48] W. Li, K.L. Wang, S.J. Cheng, K. Jiang, *Energy Storage Mater.* 15 (2018) 14–21.



**Xunfeng Zhou** received his Ph.D. (2008) degrees from Department of Chemistry, Fudan University. After graduation, he worked as a postdoctoral research fellow at Ningbo Institute of Materials, Chinese Academy of Sciences. He is currently a full professor at Ningbo Institute of Materials, Chinese Academy of Sciences. His research interests include graphene and electrochemical energy storage.



**Xiujuan Wei** received her B.S. degree from Department of Material and Chemical Engineering, Zhengzhou University of Light Industry in 2013. She received her Ph.D. degree from Wuhan University of Technology in 2018. Her current research involves the transitional metal chalcogenides for rechargeable batteries.



**Xuhui Yao** received his B.S. degree in Wuhan University of Technology in 2016. He is currently working toward the Ph.D. degree in Wuhan University of Technology and his current research focuses on the energy storage materials and devices.



**Ping Hu** received his Master degree from Wuhan University of Technology (WUT) in 2016. He is currently working toward the Ph.D. degree in WUT and his current research focuses on the energy storage materials and devices.



**Ting Zhu** received his Master degree from Tianjin Polytechnic University in 2016. She is currently working toward the Ph.D. degree in Wuhan University of Technology and her current research focuses on the energy storage materials and devices.



**Xuanpeng Wang** received his Ph.D. degree from Wuhan University of Technology in 2018. His current research focuses on material synthesis, control performance, device design, *in-situ* characterization of new-type zinc-ion batteries, sodium-ion batteries and potassium-ion batteries.



**Wen Luo** is an assistant professor at School of Science, Wuhan University of Technology (WUT). She carried out her doctoral research at WUT and Université de Lorraine, and she received her Ph.D. degree from WUT in 2018. Her current research focuses on advanced electrode materials for electrochemical energy storage devices.



**Chagnwei Shi** received his bachelor degree from Wuhan University of Technology (WUT) in 2014. He is currently working toward the Ph.D. degree in WUT and his research focuses on the energy storage materials and devices.



**Kwadwo Asare Owusu** received his Master degree from Wuhan University of Technology in 2016 and is currently working towards the Ph.D. degree under the supervision of Prof. Mai Liqiang. His research focuses on the design and synthesis of carbon/metal oxides nanomaterials for high energy density storage devices.



**Liqiang Mai** is Chang Jiang Scholar Chair Professor of Materials Science and Engineering at Wuhan University of Technology (WUT). He received his Ph.D. from WUT in 2004 and carried out his postdoctoral research in Prof. Zhonglin Wang's group at Georgia Institute of Technology in 2006-2007. He worked as an advanced research scholar in Prof. Charles M. Lieber's group at Harvard University in 2008-2011 and Prof. Peidong Yang's group at University of California, Berkeley in 2017. His current research interests focus on new nanomaterials for electrochemical energy storage and micro/nano energy devices.



**Liang Zhou** received his Ph.D. (2011) degrees from Department of Chemistry, Fudan University. After graduation, he worked as a postdoctoral research fellow at Nanyang Technological University (2011–2012) and The University of Queensland (2012–2015). He is now a full professor at Wuhan University of Technology. His research interests include functional nanomaterials for electrochemical energy storage.